Microwave-Assisted Synthesis of Zinc Sulfide Nanoparticles from s-benzyl-β-n-(4-hydroxy-3-methoxybenzylidene)dithiocarbazate Metal Complex and DFT Studies

*Aftab Alam[1],
D. Kumar[1],
Arvind Kumar[1],
Bhupendra Singh Kushwah[1,]
[1]Centre of Research for Chemical Sciences, Govt. Model Science College, Jiwaji University Gwalior M.P. 474009 India.

Rayees A. Bhat[2],
[2]Department of Chemistry, Babasaheb Bhimrao Ambedkar University (A Central University), Lucknow-226025, India

Abstract:- In this paper, we have reported highly luminious Zinc sulphide nanoparticles grown by microwave irradiated single molecular precursors. The Schiff base S-benzyl-β-N-(4-hydroxy-3-methoxybenzylidene)dithiocarbazate (ligand-IV) obtained from S-benzyl dithiocarbazate (SBDTC) and 4-Hydroxy-3-methoxy benzaldehyde. The nanoparticles obtained via thermal decomposition method and were characterized by X-ray diffraction patterns, Transmission electron micrographs (TEM) for morphological analysis and U-Vis spectra for optical analysis. X-ray diffractograms exhibit mixed structures analysis (Wurtzite and cubic) for particles obtained using 4-Hydroxy-3-methoxy benzaldehyde. The excellent optical properties of ZnS nanoparticles signify the role of microwave irradiation in synthesis. Photolumininescence (PL) study shows the luminescence in visible region and intensity is maximum for ZnS particles obtained by Zinc complex of dithiocarbazate. The microwave-assisted process can be used for large-scale production of nanoparticles for emitting light in the visible region in various detecting and sensing applications. Density functional calculations of ligand-IV in gas phase were performed by using DFT (RB3LYP) exchange correlation functional and 6-311++G (d, p) basis sets level. The computed parameters were chemical hardness (ŋ) 0.06111 eV, chemical potential (μ) -0.14048 eV, electron affinity (A) 0.07938 eV, softness (S) 16.36 eV, ionization energy (I) 0.20159 eV, electronegativity (χ) 0.14048 eV, comparative stabilization energy 0.1222 eV. HOMO energy-0.20159, LUMO energy -0.07938.

Keywords*: *Zinc Sulfide, DFT, Nanoparticle, Mep, Ditiocarbazate.

I. INTRODUCTION

Due to unique properties of Nanostructure-based semiconductor materials show significant applications for several technologies. Wurtzite phase ZnS have much better optical properties then cubic. Quantum size and surface effects play important role for advanced applications in thin film based electronics devices, IR windows, light-emitting diodes, displays, sensors, flat panel displays, catalytic applications electroluminescence [1–13]. NPs of ZnS is an important material due to its chemical stability with potential applications in absorption studies, optoelectronics, photocatalysis luminescence[14–17]. Due to wide band gap (~3.6 eV), ZnS NPs show high refraction index, and high transmittance in the visible range [18]. In recent years for the synthesis of ZnS nanostructures many synthetic routes have been developed like liquid microwave irradiation [19], reverse micelles [20], these are the Physical methods and various chemical methods and hydrothermal techniques [23] chemical vapour deposition [21], solid-liquid chemical reactions under co-precipitation [22], ZnS NPs have luminescence activity with wide band gaps has been investigated for a long time [24]. These type of measurements give information about the higher positions of the electronic states in the gap [25]. ZnS is a photoluminescence [26], thermo-luminescence [27], electro-luminescence [28] and optical absorption [29]. In recent years the use of semiconductors as fluorescence scrutiny has increased in different areas such as engineering, medicine and chemistry procedures. In our ongoing research novel Schiff base derived by the condensation method of S-benzyl dithiocarbazate and 4-Hydroxy-3-methoxy benzaldehyde in 1:1 ratio also synthesis of ZnS nanoparticle synthesis by irradiation method followed by computational studies by DFT methods at several basis sets using Gaussian 09 package [30-31].

- *Instrument Used:*

Electrical stirrer, water bath, ultrasonicator, microwave oven, electrical weighing balance, vacuum pump, separating funnel, melting point apparatus measuring within a range of 0-400 ^{0}C.

II. MOLECULAR PRECURSOR SYNTHESIS

- *Synthesis Of S-Benzyl Dithiocarbazate:*

The synthesis of SBDTC precursor was obtained via previously reported method[1]. 11.4g (0.2 mole) of KOH dissolved in (9:1) 70 ml absolute ethanol and then 10g (0.2 mole) of 100% hydrazine hydrate (NH_2-NH_2) was added to already cooled alcohol-water cooled solution slowly with constant stirring. Another solution of CS_2 15.2g (0.2 mole) is prepared by adding in 12.5 ml ethanol was added drop wise via a dropping funnel to the mixture, while the mixture was still being kept in the ice both and one hours constant stirring for vigorous mixing of solution was by mechanical stirrer. After continuous stirring two layer formed with lower yellow oily layer were separated by separating funnel, and was later dissolved in 12ml cold 40% absolute ethanol maintained at 5-7℃. The mixture was kept in an ice bath, again and 28.5g (0.2mole) of benzyl chloride with vigorous stirring continued for 30 minutes more. The milky mixture formed was then filtered and was with water and finally left to dry over silica gel. Yield: 74%, M.P : 122℃.

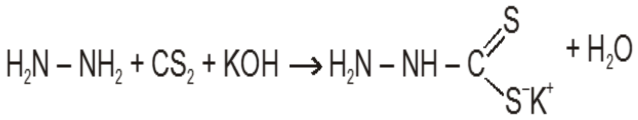

$$H_2N-NH_2 + CS_2 + KOH \rightarrow H_2N-NH-C(=S)S^-K^+ + H_2O$$

Structure of Potassium Salt of Dithiocarbazic Acid

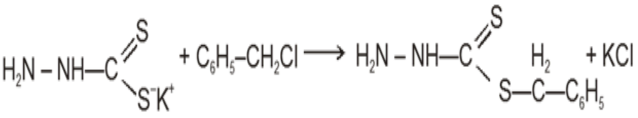

$$H_2N-NH-C(=S)S^-K^+ + C_6H_5-CH_2Cl \rightarrow H_2N-NH-C(=S)-S-\overset{H_2}{C}-C_6H_5 + KCl$$

Structure of S-Benzyl Dithiocarbazate

- *Synthesis of Schiff Base:*

The novel dithiocarbazate Schiff base were obtained by the simple condensation reaction between 4-Hydroxy-2-methoxy benzaldehyde and S-benzyldithiocarbazate (SBDTC) by 1:1 ratio 1.98g (0.01 mol) were dissolved in hot ethanol (25ml) and then heated on a heating plate with constant stirring in order to ensure the complete dissolving of the SBDTC. Similarly, 1.522g (0.01 mol) of 4-Hydroxy-2-methoxy benzaldehyde was mixed with 25 ml of absolute ethanol. This was added to a solution of metal (0.00 mole) in methanol (13ml) in 1:2 molar ratio. The resultant solution becomes coloured. The mixture was heated on water bath and refluxed for 48 minutes, when crystals started appearing. Then refluxing was stopped and the reaction mixture was allowed to stand overnight where coloured crystals formed. Precipitate was filtered off and the complex was purified by recrystallization from ethanol and dried in vacuum oven anhydrous CaCl2 in a desiccator.

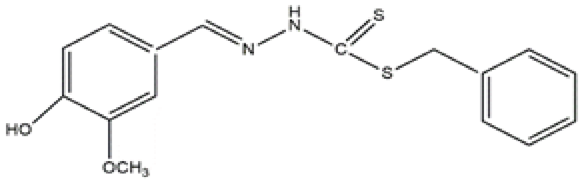

Fig 1 S-Benzyl-β-N-(4-Hydroxy-2-Methoxybenzylidene)Dithiocarbazate

- *Synthesis of Zinc (II) Complexes:*

The Schiff bases 3.324g (0.002 mol) were dissolved in hot methanol (25 ml). This was added to a solution of zinc metal salt 1.098g (0.001 mol) in methanol (20 ml) in 2:1 molar ratio. The resultant solution becomes coloured. The mixture was heated on a water bath and Refluxed for 45 minutes, when crystal of metal complexes started appearing. Then refluxing was stopped and the reaction mixture was allowed to stand overnight, whereupon coloured crystal were formed. Precipitate was filtered off and the complex was purified by recrystallization from ethanol and dried in vacuum over anhydrous $CaCl_2$ in a desiccator.

III. CHARACTERIZATION OF S-BENZYL-β-N-(4-HYDROXY-3-METHOXY BENZYLIDENE) DITHIOCARBAZATE: Ligand-IV

- *FTIR and Raman Spectral Analyses Of Ligand-IV:*

FTIR spectra (4000–400 cm^{-1}) were obtained as KBr pellet using FTIR-105627 Perkin-Elmer spectrophotometer and Raman analyses by (JYH LABRAM-HR visible spectrophotometer) present in Table: 1

Table 1 FTIR and Raman Spectral Bands of Ligand-IV

S.No	FTIR Band (cm^{-1})	Assignments
1.	3370	OH stretching vibration
2.	1609	N-H stretching vibration
3.	2917	C-H stretching vibration
4.	1669	C=N stretching vibration
5.	1506	N-N stretching vibration
6.	1358	C-N stretching vibration
7.	1360	C=S stretching vibration
8.	1228	C-O-C stretching vibration

9.	1080	N-C-S stretching vibration
10.	1037	C-S-C stretching vibration

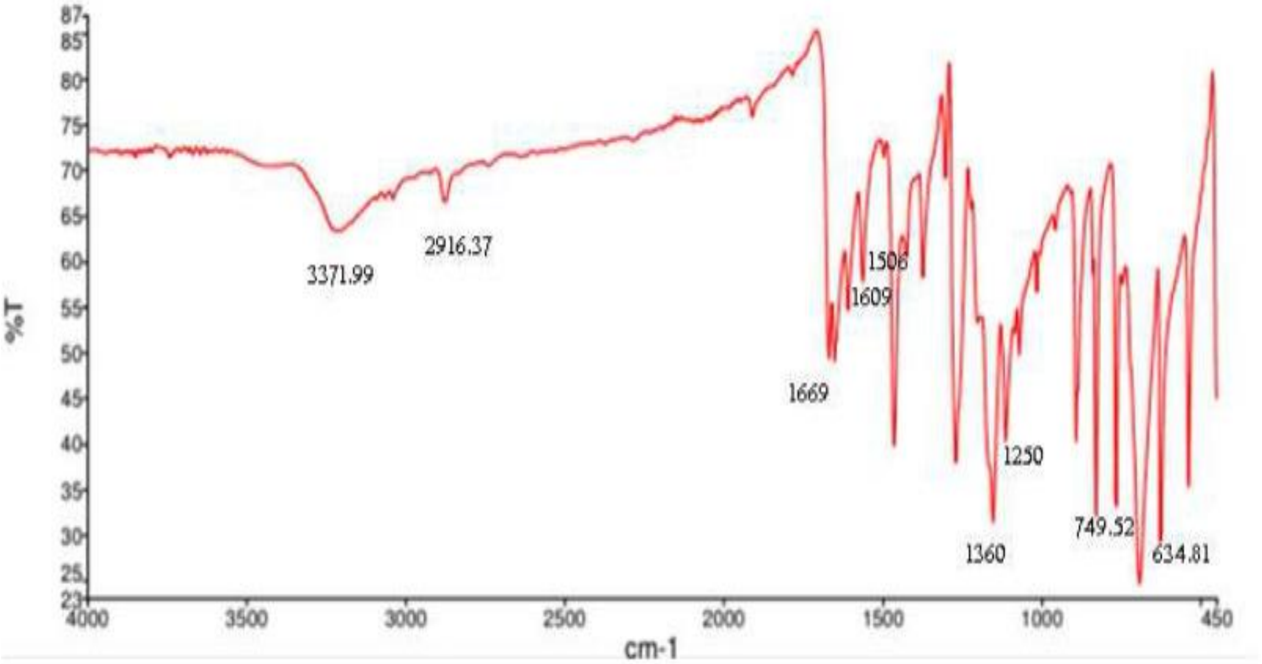

(a)Experimental

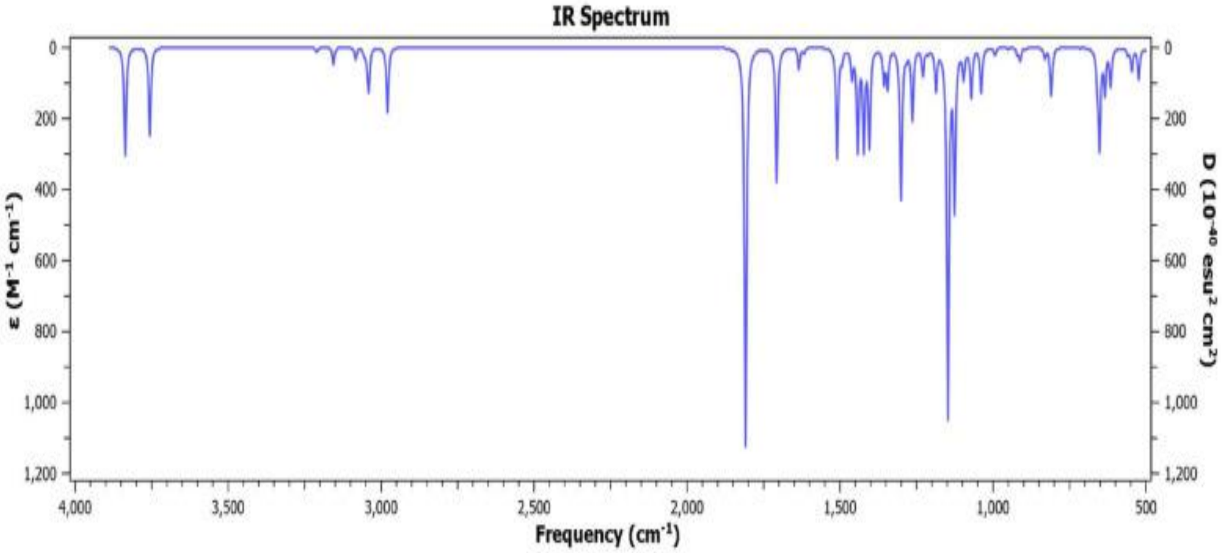

(b) Simulated

Fig 2 a) Experimental and b) Simulated

- *^{1}H NMR Spectral Analyses of Ligand:*

^{1}H-NMR (500 MHz, $CDCl_3$, ppm) δ: 5.35 (OH)1.36 (s, CH_3), 3.3 (s, SCH_2), 7.87 (s, CH), 7-7.5(m, H-ar), 2.0 (s, NH), shown in (Fig 3).

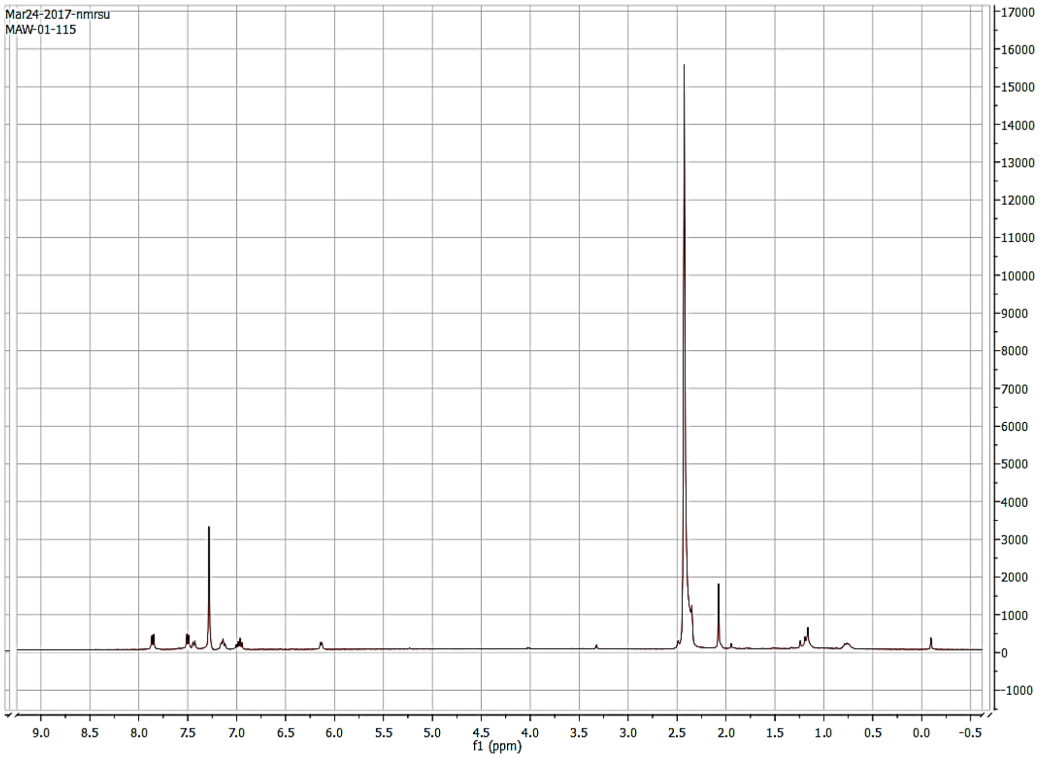

Fig 3 ^{1}H-NMR Spectra of Ligand-IV

- *Thermogravimetric Analyses of Ligand:*

TGA-50 SHIMADZU-00652 instrument was used for thermal gravimetric analysis (TGA) measurement of the ligand-IV at heating rate of 10^{o}C/min under nitrogen atmosphere shown in (Fig. 4.5). The TGA curve of the ligand-IV exhibit three random weight loses. The first estimated weight loss of 54.56% is attributed at 210℃ to C_7H_7S molecule as a gas in the second and third stages of the compound exhibits weight loss of 26.75 and 18.69% decomposition as gases at 360℃ and 643 ℃ finally residue (ash).

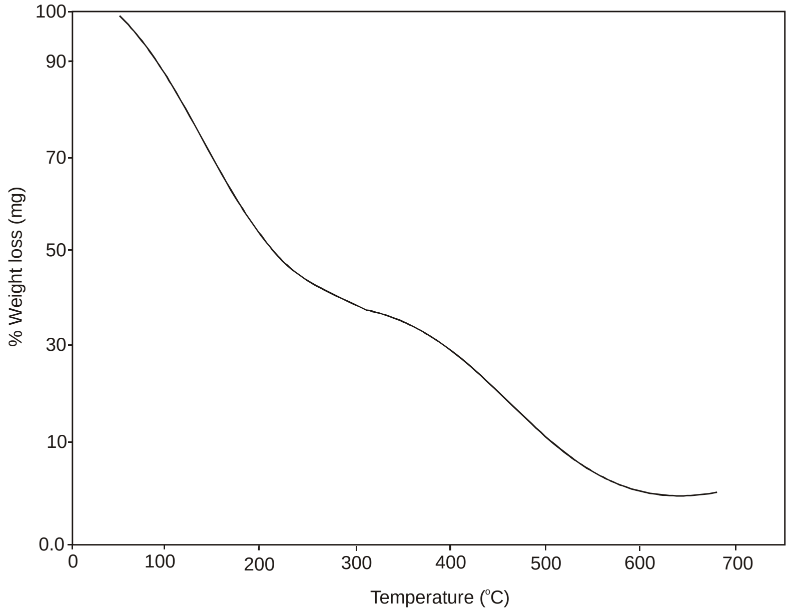

Fig 4 U.V- TGA Spectrum of ZnS Nanoparticles

- *Synthesis of Nanoparticle:*

Ultrasonication is used for obtaining ZnS nanoparticles, 1g of the zinc complex was dissolved in 25ml in DMSO in a round bottom flask. A ultrasonic treatment (using piezoelectric sandwich transducer at 40 kHz resonant frequency) was given for 30 min at 78^{o}c to it thoroughly and then kept for 35 min.Microwave irradiation Final product was heated in microwave oven for 10 min with 800 W power microwave resulted suddenly formation of ZnS nanoparticles. The solution containing particles was then cooled, centrifuged and washed with absolute methanol several times.

- *Characterization:*

Nanoparticles were collected and analysed by morphological, structural and optical characterizations. SEM and HRTEM micrographs were obtained by TECHAI G2F20 operated at 300 KV using a drop of suspension of the sample in ethanol on carbon coated copper grid. Powder X-ray diffraction patterns were obtained from using X Pert Pro PAN analytical X-ray diffractometer in the 2θ ranging from 20 to 80℃ with CuKα radiation of wavelength 1.54A^0. Optical spectra of the ZnS structures on quartz in the range 200-900 nm were obtained using Perkin Elmer Lambda 25 spectrophotometer. Photoluminescence spectra were obtained using Perkin Elmer PL-55 with excitron at 300 nm.

IV. RESULTS AND DISCUSSION

Yellow coloured ZnS nanoparticles were obtained within a short reaction times using microwave heating in DMSO. Microwave irradiated material are of high quality as microwave irradiation provides selective, rapid and uniform heating high reaction rate, and low-energy consumption. It also helps to deliver energy into the reaction vessel and accelerates the reaction kinetics and efficiency. The microwave heating reduces the crystallization time and improved the crystallinity of the final product in a better way. In our case, it helps to obtain good quality nanorods. The DMSO solvent also plays a very significant role in nanoparticle rod synthesis. DMSO has very high (0.825) value of loss tangent (tan δ) and hence at a specific frequency, efficiently convert electromagnetic radiations into heat energy. Dimethyl sulphoxide having high permanent dipole moment and boiling point is an excellent absorber of the microwave radiations, which take energy from the microwave region and heats polar reaction solution instantaneously [17,18]. The polar solvent acting both reaction media and dispersion media, thus efficiently absorb and stabilize the surface of the particles and produce monodispersed ZnS nanoparticle rods [19]. The short reduction time results in increasing product purity by minimising surplus side reactions compared to conventional heating methods. Microwave reactors allow easy access to high temperature and pressures. Structural, morphological, and optical studies were performed on the samples.

- *Optimized Geometry:*

The geometrical parameters such as dihedral angle bond length and bond angle are presented in Table 2. it can be predicted from From Table 2, that if dihedral angles allied with 4-adajacently bonded atoms are approximately equal to 0^0 or 180^0, it means accompanying atoms lie virtually in the same plane. Keeping this point under consideration the entire geometry is with two planes (plane I & II). The C=C on an average is 1.39 A^0 for double and 1.51 A^0 for single bond however, bond angle C1-C2-C3=120^0, C19-C20-C21=120^0, and C13-S15-C16= 102.7^0 . The dihedral angle for N8-N9-C13-S15 =0.000 suggests that these atoms lie almost in the same plane (Plane II) and the benxyl group lies in another plane (Plane I). The mutual intersection of two planes pass through S15 and plane 1 and 2 are inclined at an obtuse angle of 102.7. Optimized geometry results like bond length, bond order, dihedral angle are in good conformity with previously reported Schiff bases from dithiocarbazate and cinnamaldehyde crystal data [32,33].

V. X-RAY DIFFRACTION ANALYSIS OF ZINC SULFIDE

The analysis of x-ray pattern The x-ray spectra pattern shows three different peaks of the sample correspond to the lattice planes of (111), (220) and (311) which shows best comformity with the cubic zinc blende structure shown in Fig. 4 which signifies that ZnS sample crystallize in cubic symmetry (*F*-43*M* space group) with lattice parameter a = 5.368(4) Å and unit cell volume V = 154.7157(8) Å^3. The significant broad peaks of the XRD pattern reveals the small particle (crystallite) size and indicates the Nano metric particle size. The average particle size is approximately estimated by Hall’s method.

$$\frac{\beta\cos\theta}{\lambda}=\frac{1}{D}+\frac{2\varepsilon\sin\theta}{\lambda}, \qquad (1)$$

Here θ is the diffraction angle of the Bragg peak, λ = 1.54056 Å is the wavelength of the used x-ray, β is the full width at half maximum (FWHM) of that peak in radian, ε is the effective residual strain and D is the particle size. In this way D and ε can be estimated from the intercept of the β cos θ/λ axis and the slope of the curve by plotting the β cos θ/λ versus sin θ/λ respectively and regular particle size of about 5.5 nm is obtained. A dislocation is the crystallographic defect that strongly affects many properties of zinc sulphide, thus dislocation density is also calculated from the following relation:

$$\delta=\frac{15\varepsilon}{aD}. \qquad (2)$$

The effective strain and also the dislocation density are estimated to be 6.71 × 10^{-3} and 3.41× 10^{15}, respectively.

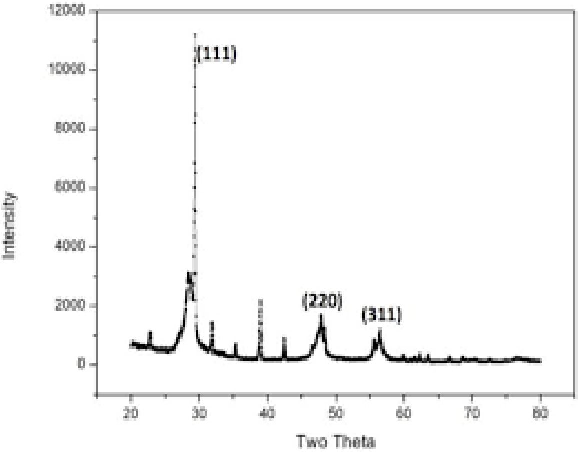

Fig 5 X-Ray Diffraction for ZnSnanoparticals

- *Scanning Electron Microscopy:*

The SEM microstructural analysed images shown in Fig 6 signifies that the synthesized ZnS contains generally the grains of ZnS particles (crystallite) with usual shape. One can see that nearly spherical nanoparticles have an almost homogenous size distribution with a mean size of 50 nm. In the absence of EDTA, a bulk ZnS sample is formed (not shown here). In the synthesis process, the usage of EDTA causes the stabilization of the small particles and the inhibition of this agglomeration. Due to the presence of −COOH group in EDTA molecule which gets absorbed on the particle surface, EDTA-capped ZnS sample is formed and its maximum particle size does not exceed beyond 70 nm.

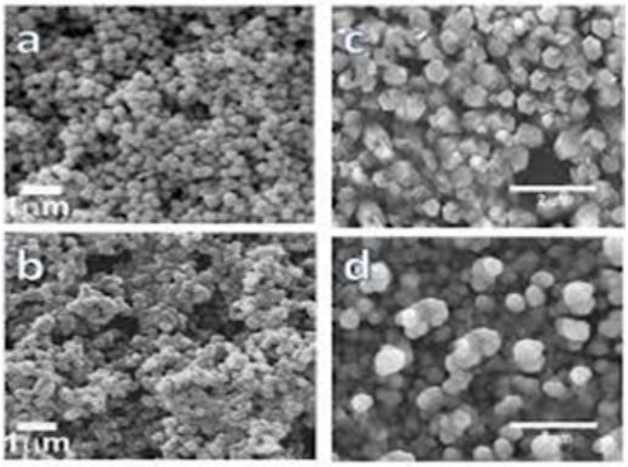

Fig 6 SEM image of ZnS Nanoparticles

- *Transmission Electron Microscopy:*

The spherical particles agglomerated with size 7.8 nm shown in TEM image of zinc sulfide depicted in Fig 7. The particles size observed in the TEM micrograph is larger than that of the crystallites estimated from the Dbye-scherrer equation.

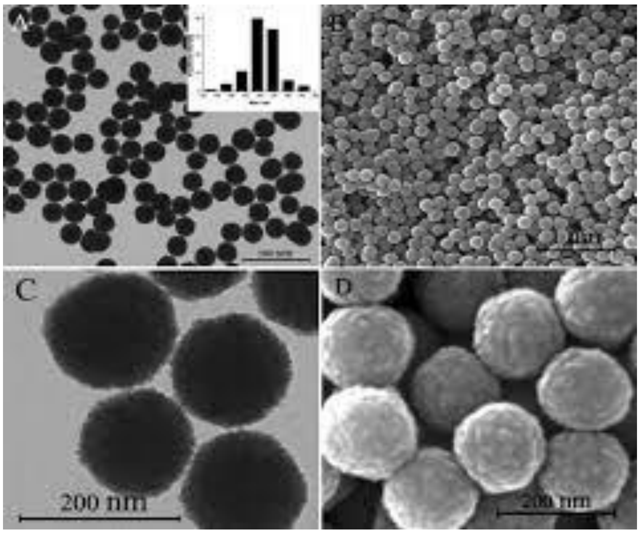

Fig 7 TEM Image of ZnS Nanoparticals

- *FT-IR Analysis:*

The distinguishing peaks of ZnS nanoparticle observed at 1540, 1102 and 617 cm^{-1}. The observed peaks at 1550–1750 cm^{-1} are attributed to the C=O stretching modes and the broad absorption peaks in a range of 3100–3600 cm^{-1} correspond to O–H stretching modes arising from the absorption of water on the surface of nanoparticles shown in Fig 8.

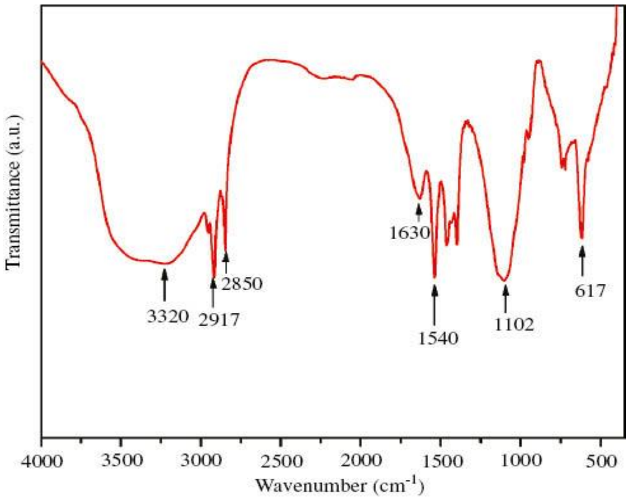

Fig 8. FTIR Spectrum of Zinc Sulfide Nanoparticles

- *UV-Visible Spectrum:*

The UV-Vis spectrum measured at room temperature shown in Fig 9 with various significant absorption modes. The strongest electronic absorption peak of the synthesized ZnS nanoparticles appears at around 245 nm.

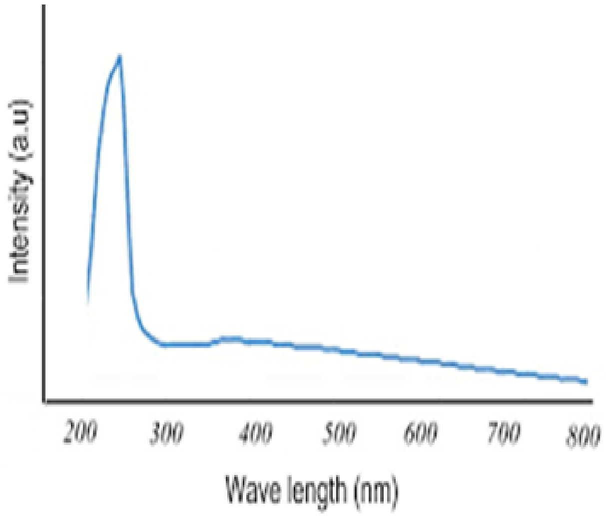

Fig 9 U.V- Visible Spectrum of Znsnanoparticals

- *Photoluminescence Spectra:*

The PL spectra of the sample are obtained for ZnS nanostructures in various excitations wavelength 425 and 452 nm in Fig. 10. The sample exhibit photoluminescence peak in the wavelength range 325-550 nm and the high intensity peak of blue emission at 325 nm have been endorsed to the Zn^{2+} vacancy related acceptor.

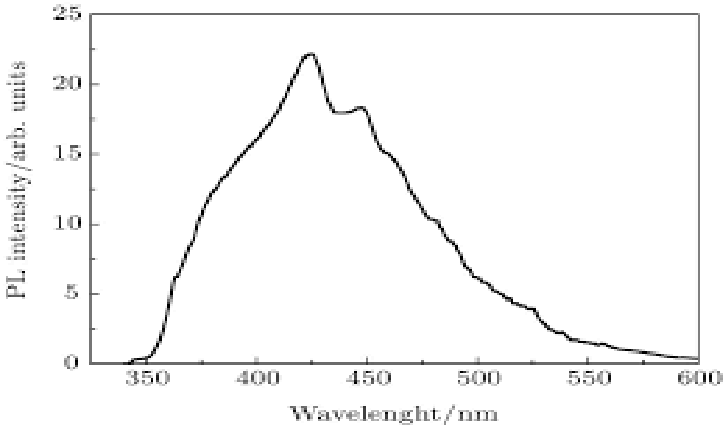

Fig 10 Photoluminescence Spectrum of ZnS Nanoparticles.

VI. DFT STUDIES

The geometrical optimization of ligand-IV were performed by density Functional Theory (DFT) method with the functional RB3LYP and basis sets 6-311++G(d,p) by Gaussian 09, Gauss View 4.1 & Veda4 software packages [34] . The Veda calculations along with PED%, HOMO–LUMO energies, MEP analysis for nucleophilic and electrophilic surface region prediction analysis of the ligand-IV by using the red and blue colour computational nomenclature, energy gaps, electronic hardness, electronic softness, analysis of Mulliken charges were calculated using RB3LYP method of the DFT [35].

Table 2 Calculated Bond Lengths, Bond Angles and Dihedral Angles of S-Benzyl-β-N-(4-Hydroxy-3-Methoxybenzylidene) Dithiocarbazate (Ligand-IV)

Bond-length (in Å)	**Bond-Angle (in ^{0})**	**Dihedral Angle (in ^{0})**
C1-C2=1.395	C1-C2-C3=119.8	C1-C2-C3-O11=179.9
C2-C3=1.391	C2-C3-O11=120.4	C1-C2-C3-C4=0.00
C3-O11=1.360	O11-C3-C4=119.9	C2-C3-C4-O11=179.9
C3-C4=1.417	C3-C4-O11=113.2	C3-C4-O10-C12=179.5
C4-C10=1.371	C4-O10-C12=118.1	C3-C4-C5-C6=0.00
O10-C12=1.424	C4-C5-C6=119.7	C4-C5-C6-C7=1.79.9
C4-C5=1.383	C5-C6-N8=121.2	C6-C7-N8-N9=179.7
C5-C6=1.413	C7-N8-N9=122.4	C7-N8-N9-C13=179.9
C6-C7=1.455	N8-N9-C13=116.9	N8-N9-C13-S14=179.9
C7-C8=1.289	N9-C13-S14=119.5	N8-N9-C13-S15=0.00
N8-N9=1.360	N9-C13-S15=112.4	N9-C13-S15-C15=179.5
N9-C13=1.359	C13-S15-C16=102.7	C13-S15-C16-C17=108.4
C13-S14=1.671	S15-C16-C17=113.6	S15-C16-C17-C19=100.6
C13-S15=1.781	C16-C17-C19=120.5	C16-C17-C13-C20=179.7
S15-C16=1.851	C17-C19-C20=120.8	C17-C19-C20-C22=0.00
C16-C17=1.508	C19-C20-C21=120.0	C19-C20-C21-C22=0.00
C17-C19=1.400	C20-C21-C22=119.7	C20-C21-C22-C18=0.00
C19-C20=1.396	C21-C22-C18=120.3	C21-C22-C18-C17=0.00

- *Mulliken Atomic Charges Analysis:*

Ligand-metal charge transfer & metal-ligand charge transfer, atomic charges, molecular behaviour, reactivity and hence analysis of atomic charges plays an important role in coordination chemistry of complexes. Mulliken population analysis gives insight regarding coordination compound formation by showing change in atomic charges before and after complex formation, similarly in ligand-IV S15 and N8 responsible for coordination with metal atom having higher negative charges, computed via DFT/B3LYP methods with 6-311++G (d, p) basis set level listed in Table 3.

Table 3 Milliken Atomic Charges of Ligand-IV Calculated by B3LYP/ 6-311G ++ (d, p) Methods.

Atom	**Charge**	**Atom**	**Charge**	**Atom**	**Charge**
C1	-0.138	O10	-0.564	S15	0.211
C2	-0.114	O11	-0.556	C16	-0.434
C3	0.306	N8	-0.270	C17	-0.132
C4	0.335	N9	-0.296	C18	-0.112
C5	-0.163	C12	-0.083	C19	-0.120

C6	0.080	C13	0.008	C20	-0.083
C7	0.111	S14	-0.246	C21	-0.085
				C22	-0.087

- *Frontier Molecular Orbital Analysis:*

Highest occupied frontier molecular orbitals (HOMO) are chemically more active and have low kinetic stability [36-39] among the frontier molecular orbitals are responsible for electrophilic and low energetic which corresponds to ionization potential and nucleophilic behaviour and high energetics, lowest unoccupied molecular orbital (LUMO) corresponds to electron affinity [40] are expressed as: A = -ELUMO and IP= -EHOMO and electronegativity(χ), chemical potential(V), chemical hardness(η), Chemical softness (S) and Electrophilicity (ω) are derived by mathematical (χ) =(IP+EA)/2, (V) = - (IP+EA)/2, (η) = (IP-EA)/2, Chemical softness (S) inverse of chemical hardness $S= 1/\eta$, Electrophilicity $\omega = V^2/2\eta$ these values are listed in Table 4 for Ligand-IV shows 0.1222 eV energy gap between two frontier orbitals (HUMO & LUMO) shown in Fig. 11.

Table 4. Calculated Frontier Molecular Orbitals Energies Values.

Parameters	HOMO(IP)	LUMO(EA)	Energy Gap	Electro-Negativity(χ)	Chemical potential(V)	Chemical Hardness(η)	Chemical Softness(S)	Electro-Philicity(ω)
Ligand-IV	-0.20159	-0.07938	0.1222	0.14048	-0.14048	0.06111	16.36	0.1615

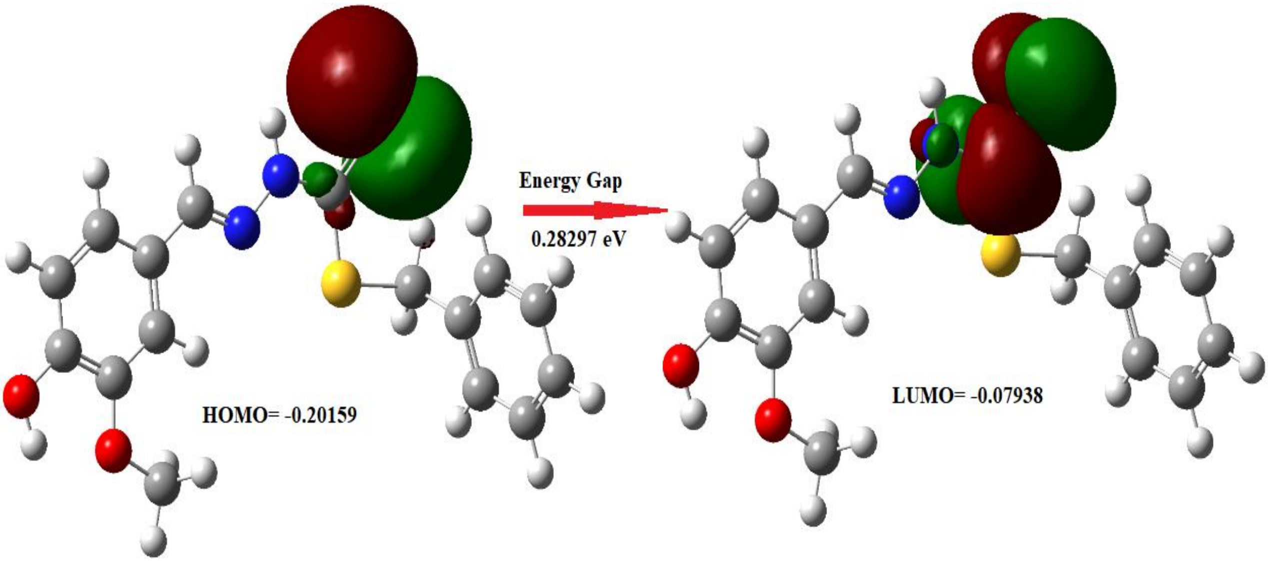

Fig 11 - 3D Plots of Frontier Molecular Orbitals of Ligand-IV

- *Molecular Electrostatic Surface Potential (MESP Analysis):*

The molecular electrostatic potential (MEP) maps or molecular electrical potential surfaces or electrostatic potential energy maps are accountable for the chemical behavior like chemical bonding, electronegativity, chemical potential, HOMO-LUMO energy gap, chemical hardness, chemical softness, ionization energy, electron affinity of molecular system and these maps are created by nuclei and electrons at specific points i,e electronegative and electropositive portions with different colors coded in map according to specific potential in Fig 12 Region with low potential or higher than average electrostatic potential energy has strong influence of positively charged particles and vice versa. Reactivity towards positive and negative charged regions can be forecasted through pictorial illustration by quantum-chemical simulations [41]. The substantial positive potential and electron deficient coded in the form of light blue color lie mainly on the terminated hydrogen atoms attached to N, aldehydic carbon and benzene carbon atoms however, the S, N and C atoms having yellow and green color of ligand IV are under intermediary potential regime.

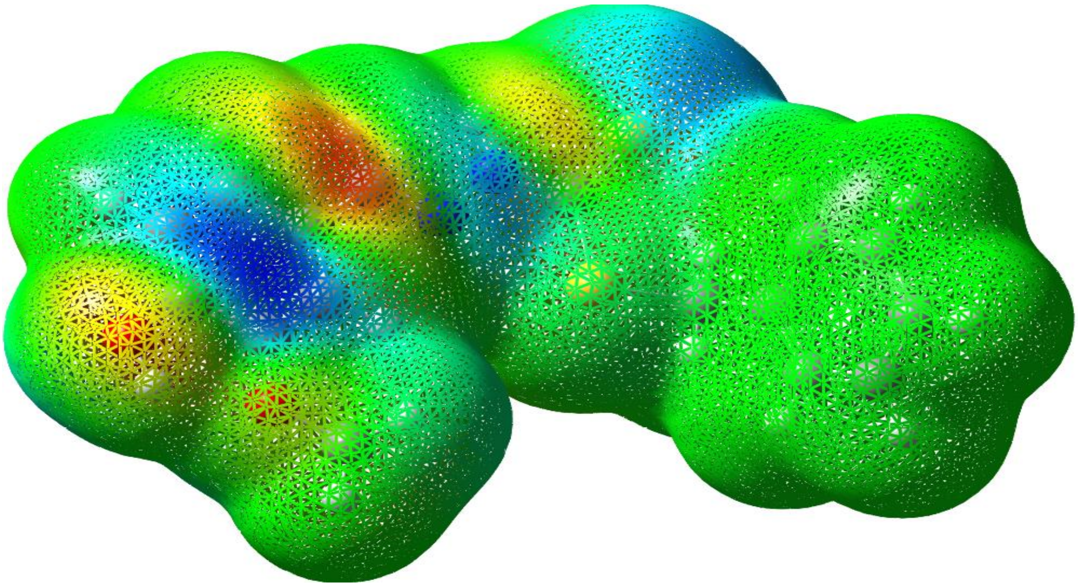

Fig 12- 3D Plots of MEP of Ligand-IV

VII. CONCLUSION

ZnS nanoparticles are successfully synthesized by using microwave irradiation of S-benzyl-β-N-(4-hydroxy-3-methoxybenzylidene)dithiocarbazate (ligand-IV) as a single molecular source precursor. The use of DMSO for microwave irradiation help to decompose precursor very fast in the form of chemical bonding and structural properties of sample are characterized by FTIR and x-ray diffraction to identify the chemical system morphology and crystal structure. The x-ray diffraction pattern indicates the very good cubic zinc-blended structure of ZnS nanocrystals. The SEM image reveals that the ZnS nanoparticles have regular shapes with an average size of 50 nm. TEM images disclose the spherical shape of ZnS nanoparticles with an average particle size is 7.8 nm. The UV spectrum of ZnS nanoparticles shows the strong quantum confinement effect with a blue shift in the band gap energy due to the nanocrystallineZnS particles. Excellent PL spectrum consists of 425- and 452-nm emission bands. The ligand S-benzyl β-N (4-hydroxy-3-methoxy benzylidene) dithiocarbazate was prepared by condensation method from S-benzyl dithiocarbazate with 4-hydroxy-3-methoxybezaldehyde in 1:1 ratio and its morphology was characterized by FT-IR, UV-Vis, ^{1}H NMR, Raman and ESI+-mass spectroscopic techniques. The opimized structure of ligand-IV and their structural parameters simulated by DFT with B3LYP exchange correlation functional in combination with 6-311++G (d, p) basis sets. The chemical hardness of compound is (η) 0.06111 eV, softness (S) 16.36 eV, ionization energy (0.20159) eV, electron affinity (0.07938) eV, electronegativity (0.14048) eV, Both Experimental and calculated results were in good conformity. The molecular electrostatic potential (MESP), stabilization energies values along with the complete investigation of both Raman and vibrational spectra was also used to access structural and symmetry properties of the studied molecule.

REFERENCES

[1]. M.Khalkhali, Q.Liu, H. Zeng, H.Zhang. Sci. Rep. 2015; 5: 14267.

[2]. R.Bhadra,V.N.Singh, B.R.Mehta, P.Datta, Chalcogenide Lett. 2009; 6(5): 189–196.

[3]. D.Ayodhya, M.Venkatesham, A.S. Kumari, G.B.Reddy, D. Ramakrishna, G.Veerabhadram ,J. Fluoresce. 2015; 25(5): 1481–1492.

[4]. D.Ayodhya, G.Veerabhadram, Superlattices and Microstructures. 2017; 102: 103– 118.

[5]. D. Ayodhya,G.Veerabhadram,J. Photochem. Photobio. B: Biology. 2016; 157: 57–69.

[6]. D.Ayodhya,M.Venkatesham, A.S. Kumari, G.B.Reddy, D.Ramakrishna,G.Veerabhadram, J. Exp. Nanosci. 2016; 11(6): 418–432

[7]. H.Emadi, M.Salavati-Niasari, A.Sobhani, Advances in Colloid and Interface Science. 2017; 246:52–74.

[8]. [8] D. Ghanbari, M.Salavati-Niasari,J. Indus. Eng. Chem. 2015; 24: 284–292.

[9]. M. Mousavi-Kamazani, M.Salavati-Niasari, M.Goudarzi, Z. Zarghami,J. Molecular Liquids. 2017; 242: 653–661.

[10]. M.Mousavi-Kamazani, Z. Zarghami, M. Salavati-Niasari,J. Phys. Chem. C. 2016; 120(4): 2096– 2108

[11]. M. Sabet, M.Salavati-Niasari, O.Amiri, ElectrochimicaActa. 2014; 117: 504–520.

[12]. H.Safardoust-Hojaghan, M. Shakouri-Arani, M. Salavati-Niasari,Transactions of Nonferrous Metals Society of China. 2016; 26(3): 759–766.

[13]. D. Ayodhya, G. Veerabhadram, J. Environ. Chem. Eng. 2018; 6: 311–324

[14]. R. Yi, G. Qiu, X. Liu, Rational bes. J. Solid State Chem. 2009; 182: 2791– 2795.

[15]. M. Kaur, N.K. Gupta, C.M. Nagaraja,Cryst. Eng. Comm. 2015; 17: 2359–

[16]. H.R.Rajabi, M. Shamsipur,A.A.Khosravi,.O. Khani, M.H. Yousefi, SpectrochimicaActa Part A: Molecular and Biomolecular Spectroscopy. 2013; 107: 256–262.

[17]. [17] M. Shamsipur, H.R. Rajabi, Mater. Sci. Eng. C. 2014; 36: 139–145.

[18]. [18] F.A. La Porta, M.M. Ferrer, Y.V. De Santana, C.W. Raubach, V.M. Longo, J.R.Sambrano, E. Longo, J. Alloy. Compd. 2013; 556: 153–159.

[19]. J. Zhu, M. Zhou, J. Xu, X.Liao, Mater. Lett. 2001; 47: 25–29

[20]. P.S. Khiew, S. Radiman, N.M. Huang, S.M. Ahmed, K. Nadarajah,Mater. Lett. 2005; 59: 989– 993.

[21]. V.G. Bessergenev, E.N. Ivanova, Y.A. Kovalevskaya, S.A. Gromilov, V.N. Kirichenko, S.M. Zemskova, I.G.Vasilieva, B.M. Ayupov,N.L. Shwarz, Mater. Res. Bull. 1995; 30: 1393–1400.

[22]. D. Ayodhya, M. Venkatesham, A.S. Kumari, K.G. Mangatayaru, J. Appl. Chem. 2013; 6(1): 1–9

[23]. J.Liu, J. Ma, Y. Liu, Z.Song, Y. Sun, J. Fang, Z. Liu, J. Alloys Compd. 2009; 486: L40–L43.

[24]. D. Denzler, M. Olschewski, K. Sattler, J. Appl. Phys. 1998; 84: 2841–2845.

[25]. H. Sasakura, H. Kobayashi, S. Tanaka, J. Mita, T. Tanaka, H. Nakayama, J. Appl. Phys. 1981; 52: 6901–6906.

[26]. J. Huang, Y. Yang, S. Xue, B. Yang, S. Liu Shen, J. Appl. Phys. Lett. 1997; 70: 2335–2337.

[27]. R. Sharma, D.P.Bisen. Luminescence. 2015; 30(2): 175–181.

[28]. D.R. Frankl, J. Phys. Rev. 1958; 111: 1540–1549

[29]. W. Chen, Z. Wang, Z. Lin, L. Lin, J. Appl. Phys. 1997; 82: 3111–3115.

[30]. D. Ayodhya, G. Veerabhadram, Mater. Sci. Eng. B. 2017; 225: 33–44.

[31]. K.Rurack, U.R. Genger, Rigidization, Chem. Soc. Rev. 2002; 31: 116–127.

[32]. E.N.M. Yusof, M.I.M. Tahir, T.B.S.A. Ravoof, S.L. Tan, E.R.T. Tiekink, Acta Cryst. E. 73 (2017) 543e549.

[33]. Y.H. Liu, J. Ye, X.L. Liu, R. Guo, J. Coord. Chem. 62 (2009) 3488e3499.

[34]. R.A. Bhat, D. Kumar, Res. on Chem. Inter. https://doi.org/10.1007/s11164-019-03752-0 (2019).

[35]. R.A. Bhat, D. Kumar, K. Singh, A. Srivastava, Md. S. Khan, M.A. Malla, J.A. Ganie, M.A. Mir, J. Mol. str. 1199 (2020) 126877.

[36]. N. Sinha, O. Prasad, V. Narayan, S.R. Shukla, J. Mol. Simul. 37 (2011) 153e163.

[37]. F.V. Lewis, C. Loannides, D.V. Parke, Xenobiotica 24 (1994) 401e408.

[38]. B. Kosar, C. Albayrak, Spectrochim. Acta. A. 78 (2011) 160e167.

[39]. M.J. Alam, S. Ahmad, Spectrochim. Acta. A. 136 (2015) 961e978.

[40]. T.A. Koopmans, Physica 1 (1934) 104e113.

[41]. R.A. Bhat, D. Kumar, M. A. Malla, S. U. Bhat, M. S. Khan, O. Manzoor, A. Srivastava, R. A. Naikoo, M. Mohsin, M.A. Mir. J. Mol. str 1156 (2018) 280-289.